Supporting Information

Enhanced NH_3 Uptake and Selectivity at low pressure in Monolithic MOF-808 Metal-Organic Gels Incorporating $CuCl_2$

Chuan Zhou[a, 1], *Feng Liu*[a, 1], *Chao Zheng*[a], *Qiong Wu*[a], *Hantong Chen*[a], Liangyu Li[b], Jiayu Zhai[a], Li Li[a,*], *Bo Yang*[a,*], *Pingwei Ye*[a,*]

a. State Key Laboratory of Chemistry for NBC Hazards Protection, Beijing 102205, PR China
b. Yichang Office of the Army Equipment Department, Yichang 44300, PR China

Table of Contents

1. Experimental Section ……..2
2. Figures S1-S15 …… …… 4
3. Tables S1-S2……10
4. References ……11

[*] Corresponding authors.
E-mail addresses: lily97@buaa.edu.cn (L. Li), dahema2007goodluck@163.com (B. Yang), yepw2001@163.com (P. Ye).

[1] These authors contributed equally to this work.

1. Experimental Section

Materials. All chemicals are used as received without further purification. Zirconyl chloride octahydrate ($ZrOCl_2$•$8H_2O$, 99.9%), $CuCl_2$ (99%), and *N, N*-dimethylformamide (DMF, 99.9%) are purchased from Shanghai Macklin Ltd. Trimesic acid (H_3BTC, 99%), formic acid (FA, 99%), and methanol (99.8%) are provided by Beijing J&K Scientific Ltd. Acetone (99%) is purchased from Beijing Sinopharm Chemical Ltd.

Synthesis of G808. H_3BTC (0.68 g, 3.2 mmol) is dissolved in DMF (20 ml) and FA (20 ml), followed by the addition of $ZrOCl_2$•$8H_2O$ (3.09 g, 9.6 mmol). Once a clear solution is formed, it is put into an oven and heated at 100 °C for 24 h. After cooling down to room temperature, the produced MOF-808 gel is washed with DMF, followed by freeze-drying. The white granular product is subsequently washed with acetone and methanol and then dried overnight under vacuum at 110 °C to produce MOF-808 xerogel (labeled as G808).

Synthesis of $CuCl_2$@G808. 100 mg of G808 is added to a solution containing $CuCl_2$ (1200 mg) dissolved in water (3 mL) and impregnated at 80 ℃ for 24 h. The product is collected by removing the supernatant and washed with water. $CuCl_2$@G808 is dried and activated under vacuum at 110 °C before further use. The loading of Cu in $CuCl_2$@G808 is 1.21%, as determined by inductively coupled plasma-optical emission spectrometry (ICP-OES).

Characterization. Powder X-ray diffraction (PXRD) patterns are collected using a Rigaku Ultima IV X-ray diffractometer with Cu-Kα radiation (λ = 1.5418 Å) from 2θ=3° to 50°. Thermogravimetric analyses (TGA) are determined by a Netzsch TG analyzer through heating from 30 to 800 °C under air with a heating rate of 5 ℃/ min. Fourier transform infrared (FT-IR) spectra are collected with a Thermo Scientific Nicolet iS20 spectrometer. N_2 adsorption isotherms are measured on a Micrometer ASAP 2020 analyzer at 77 K. ICP-OES analysis is performed on a Agilent 5110. The morphology of samples is observed by a ZEISS Gemini 300 field emission scanning electron microscope. In-situ FTIR spectra are recorded on a Nicolet iS50 (Thermo Fisher Scientific) spectrometer, and the spectral resolution and the number of spectral sweep cycles are

set to 4 and 32, respectively. The sample is mixed with KBr powder and pressed into a transparent sheet before use. After the sample is placed into IR cells, it is activated at 120 °C for 2 h and then cooled to room temperature. Then, NH_3 mixture (50 ppm NH_3/Ar) flows into the IR cell for in-situ IR measurements. XPS is recorded on a Thermo Scientific K-Alpha electron energy spectrometer using Al Kα (1486.6 eV) radiation as the X-ray excitation source. NH_3, N_2, and H_2 isotherms are measured using a BSD-PM gas sorption analyzer. The desolvated sample is generated in situ within the sample holder of the instrument by heating the sample to 393 K under vacuum until the sample mass has stabilized. For the cycling tests, NH_3 adsorption experiment on $CuCl_2$@G808 is conducted at 298 K for five times. After each run, the adsorbent must be heated to 393 K under vacuum to aid regeneration. Dynamic mixed gas breakthrough experiments are performed using a multi-constituent adsorption breakthrough curve analyzer (BSD-MAB) under dry condition at 298 K. $CuCl_2$@G808 is placed in a quartz column with inside diameter of 4 mm. The length of packed bed is 60 mm. The flow rate at the inlet is 13.27 cm/s. The sample mass of MOF in the packed bed is 0.6235 g. The MOF framework density is 3.8 g/cm^3. The dry helium flow (30 mL/min) with 423 K is introduced into the column for 4 h. Upon cooling, the dry gas mixture $NH_3/N_2/H_2$ (v:v:v:=3:25:72) is passed through the column. The eluted gas concentration is continuously monitored by an INFICON mass spectrometer.

Isosteric heat. Heat of adsorption profiles are calculated by fitting the Virial model on adsorption isotherms of ammonia collected at 273 K and 298 K. The fitted isotherms are analyzed with the isosteric heat of adsorption defined as **Equation 1**:

$$Q_{iso} = -\Delta_{ads}H_{diff} = \frac{R_g T_1 T_2}{T_2 - T_1} Ln\left(\frac{P_2}{P_1}\right) \qquad \textbf{Equation 1}$$

Where Q_{iso} is the isosteric heat (J·mol^{-1}); P_1 and P_2 are the absolute pressure (kPa or bar) corresponding to T_1 and T_2 arriving at the equal saturated adsorption capacity, respectively; T_1 and T_2 are the system temperature (K); R_g is the ideal gas constant (8.314 J·mol^{-1}·k^{-1}).

IAST selectivity. The single-component adsorption isotherms of NH_3, N_2 and H_2 are fitted with the dual-site Langmuir Freundlich (DSLF) model (**Equation 2**). Then the IAST selectivity ($S_{A/B}$) are calculated as **Equation 3** [1, 2].

$$n = n_1 \times (b_1 \times p)^{q1} / \left(1 + (b_1 \times p)^{q1}\right) + n_2 \times (b_2 \times p)^{q2} / \left(1 + (b_2 \times p)^{q2}\right) \qquad \textbf{Equation 2}$$

Where n is adsorption amount; n_0, n_1 and n_2 are the saturated adsorption capacities; b and q are fitting parameters including b_1, b_2, q^1 and q^2; p is pressure. The regression parameters for all of the fits are above 0.99, confirming the reliability of the modelling.

Second, selectivity calculations are performed using the Ideal Adsorbed Solution Theory (IAST) method calculated using pure component isotherm data:

$$S = \frac{x_1/y_1}{x_2/y_2} \qquad \textbf{Equation 3}$$

Where x_i is the amount of each component adsorbed and y_i is the mole fraction of each component at equilibrium.

2. Figures S1-S15

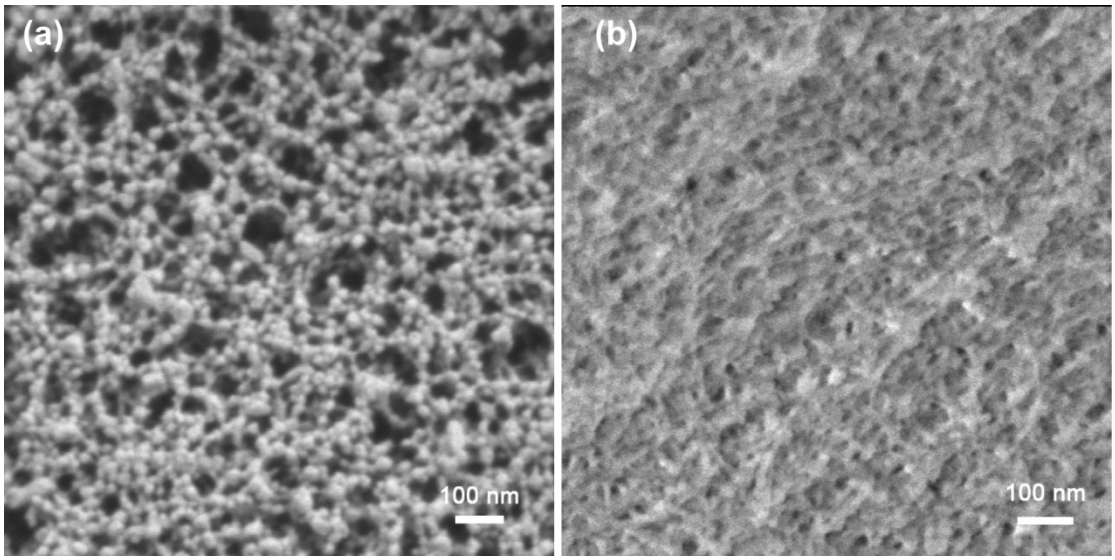

Figure S1. SEM images of (a) G808 and (b) $CuCl_2$@G808.

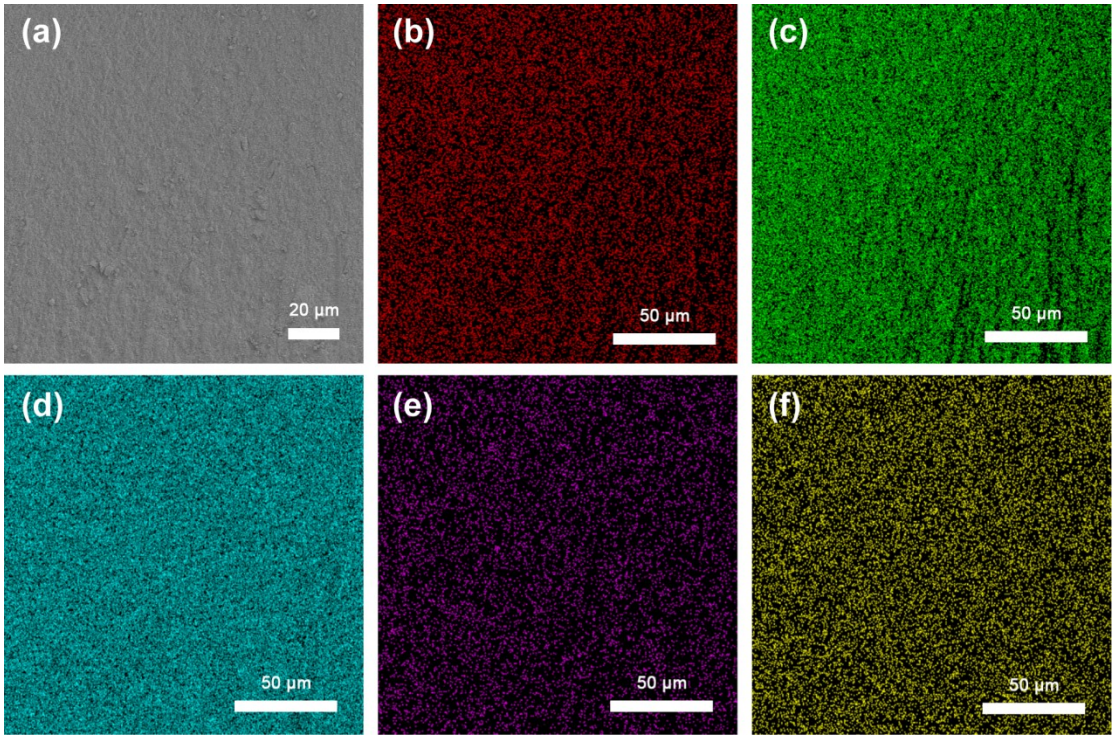

Figure S2. SEM image of (a) $CuCl_2$@G808 and its corresponding EDX elemental mapping of (b) C, (c) O, (d) Zr, (e) Cu, and (Cl).

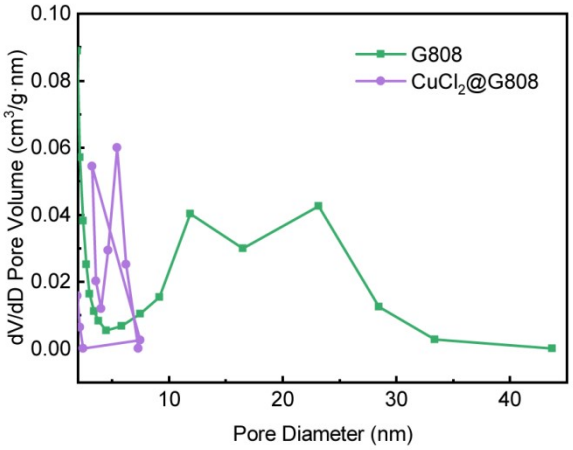

Figure S3. BJH pore size distributions of materials.

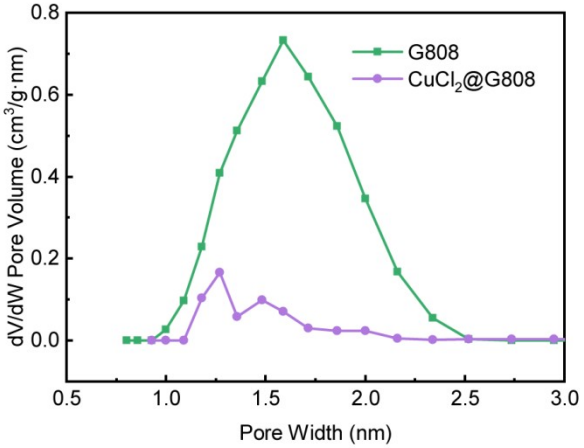

Figure S4. NLDFT pore size distributions of materials.

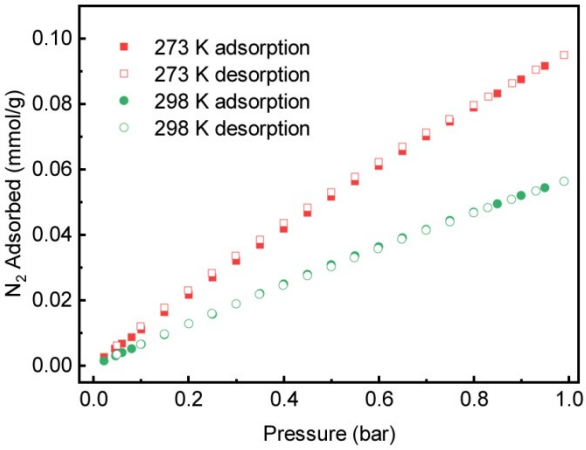

Figure S5. Sorption isotherms of $CuCl_2$@G808 for N_2.

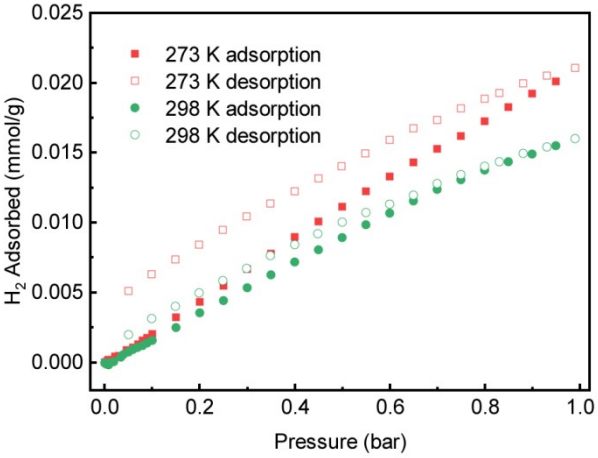

Figure S6. Sorption isotherms of $CuCl_2$@G808 for H_2.

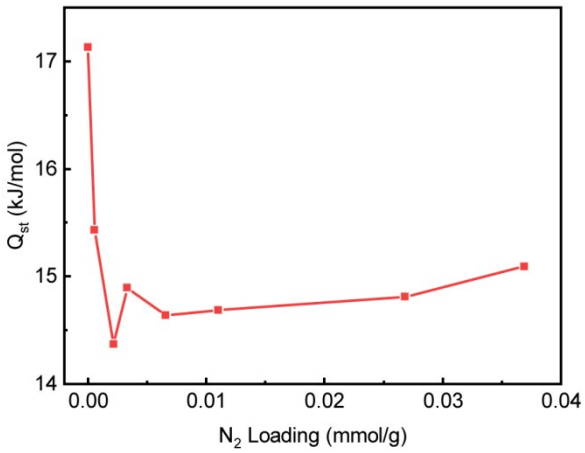

Figure S7. Isosteric heats of adsorption (Q_{st}) as a function of gas loading of N_2 in $CuCl_2$@G808.

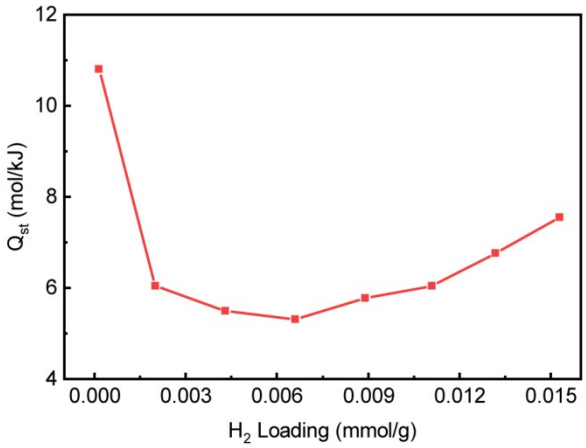

Figure S8. Isosteric heats of adsorption (Q_{st}) as a function of gas loading of H_2 in $CuCl_2$@G808.

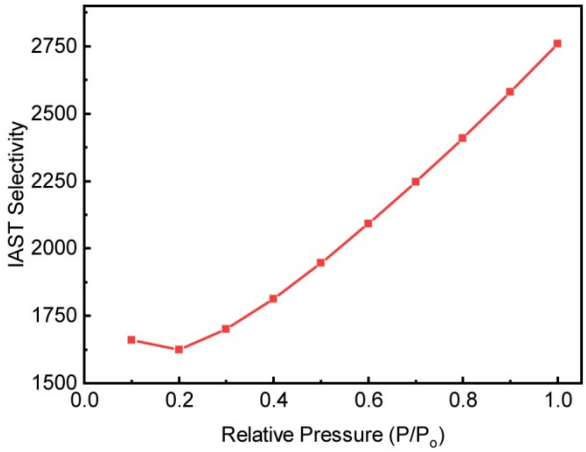

Figure S9. IAST selectivity values for NH_3/N_2 mixtures at gas ratios of 1:999 calculated from single component isotherms collected at 298 K.

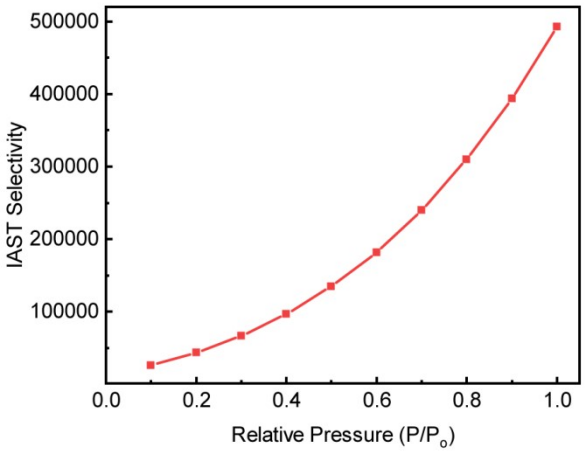

Figure S10. IAST selectivity values for NH_3/H_2 mixtures at gas ratios of 1:999 calculated from single component isotherms collected at 298 K.

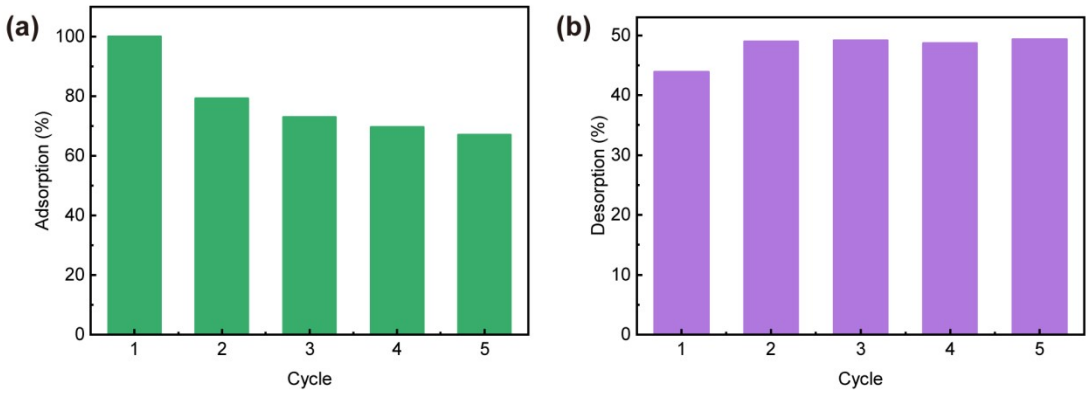

Figure S11. Cyclic adsorption-desorption of NH_3 at 298K between 0 and 1 bar.

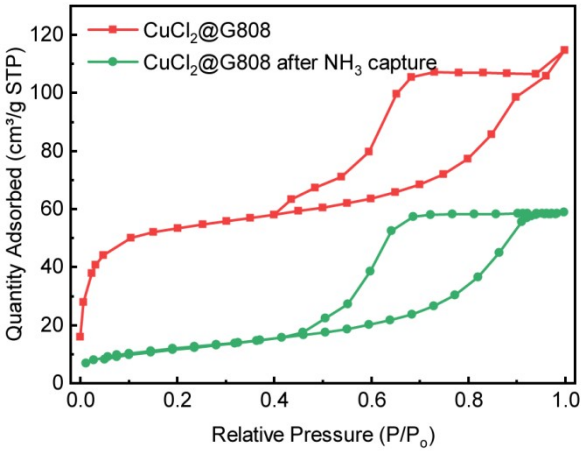

Figure S12. Nitrogen adsorption isotherms of $CuCl_2$@G808 and $CuCl_2$@G808 after five NH_3 capture cycles.

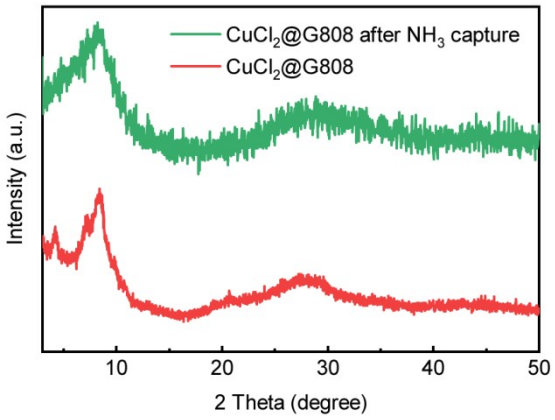

Figure S13. PXRD patterns of $CuCl_2$@G808 and $CuCl_2$@G808 after five NH_3 capture cycles.

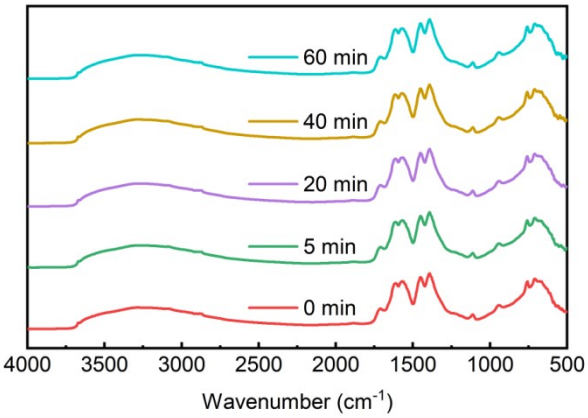

Figure S14. In situ FTIR spectra of the $CuCl_2$@G808 during NH_3 uptake.

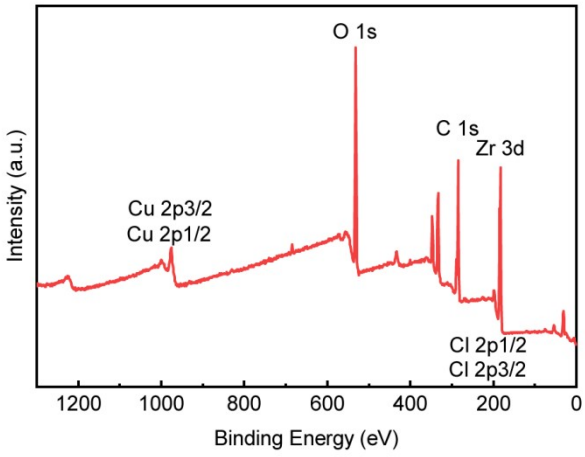

Figure S15. The XPS survey spectrum of $CuCl_2$@G808.

3. Table S1-S2

Table S1. BET area (S_{BET}), total pore volume (V_{tot}), and median pore width of samples.

Sample	S_{BET} (m^2/g)	V_{tot} (cm^3/g)	Median pore width (nm)
G808	1596.30	1.55	22.50
$CuCl_2$@G808	206.22	0.18	0.74

Table S2. Comparison of data for reported typical NH_3 adsorbents.

MOF	**NH_3 Capacity (mmol/g)**		**Stability towards Dry Ammonia**	**Reference**
LiCl@MIL-53-$(OH)_2$-43.4	1.8 (298 K 10 mbar)	33.9 (298 K 1 bar)	Reversible for 15 Cycles	[3]
LiCl@G66-OH-35.7	2.6 (298 K 1 mbar)	25.5 (298 K 1 bar)	Loss of Crystallinity	[4]
IL@MIL-101(Cr)	6.59 (298 K 0.1 bar)	24.12 (298 K 1 bar)	Reversible for 5 Cycles	[5]
Mg_2(dobpdc)	8.25 (298 K 0.57 mbar)	23.9 (298 K 1 bar)	Reversible for 3 Cycles	[6]
Ni_acryl_TMA	12.33 (298 K 0.1 bar)	23.5 (298 K 1 bar)	Reversible for 5 Cycles	[7]
Cu_2Cl_2BBTA	7.52 (298 K 1 mbar)	19.79 (298 K 1 bar)	Loss of Crystallinity	[8]
MOF-303(Al)	1.54 (298 K 1 mbar)	19.7 (298 K 1 bar)	Reversible for 20 Cycles	[9]
MOF-253(Al)-$NiCl_2$-2	5.2 (298 K 0.03 bar)	18 (298 K 1 bar)	Loss of Crystallinity	[10]
MFU-4	2.63 (298 K 1 mbar)	17.7 (298 K 1 bar)	Loss of Crystallinity	[11]
Cu(cyhdc)	0.49 (298 K 5 mbar)	17.5 (298 K 1 bar)	Decrease of Uptake	[12]
$Co(NA)_2$	1 (298 K 0.22 bar)	17.5 (298 K 1 bar)	Reversible for 3 Cycles	[13]
MFM-300(V^{IV})	1.9 (298 K 1 mbar)	17.3 (273 K 1 bar)	Reversible for 18 cycles	[14]
Cu(BDC)	1.33 (298 K 10 mbar)	17.2 (298 K 1 bar)	Reversible for 3 Cycles	[15]
UiO-66-Cu^{II}	4.15 (298 K 0.63 mbar)	16.9 (273 K 1bar)	Reversible for 15 Cycles	[16]
DUT-6-$(OH)_2$	5 (298 K 1 mbar)	16.4 (298 K 1bar)	Loss of Crystallinity	[17]
[Mn_2Cl_2BTDD]	2.72 (298 K 2 mbar)	15.5 (298 K 1bar)	Reversible for 3 Cycles	[18]
Fe-soc-MOF	3.87 (298 K 10 mbar)	14.7 (298 K 1bar)	Decrease of Uptake	[19]
MFM-300(Sc)	1.36 (298 K 10 mbar)	13.1 (298 K 1bar)	Reversible for 5 Cycles	[20]
$CuCl_2$@G808	3.65 (298 K 10 mbar)	8.1 (298 K 1bar)	Decrease of Uptake	**This work**

4. References

[1] Chang, M.; Ren, J.; Wei, Y.; Wang, J.-X.; Yang, Q.; Liu, D.; Chen, J.-F. A robust metal-organic framework with guest molecules induced splint-like pore confinement to construct propane-trap for propylene purification. Separation and Purification Technology. **2021**, 279, 119656-119663.

[2] Walton, K. S.; Sholl, D. S. Predicting multicomponent adsorption: 50 years of the ideal adsorbed solution theory. **2015**, 61, 2757-2762.

[3] Shi, Y.; Wang, Z.; Li, Z.; Wang, H.; Xiong, D.; Qiu, J.; Tian, X.; Feng, G.; Wang, J. Anchoring LiCl in the nanopores of metal-organic frameworks for ultra-high uptake and selective separation of ammonia. Angewandte Chemie-International Edition. **2022**, 61, e202212032.

[4] Zhou, C.; Sun, J.; Zheng, C.; Tao, C.-a.; Li, L.; Bai, S.; Fu, G.; Yang, X.; Zhang, S.; He, S. Monolithic UiO-66-OH metal-organic gels integrating LiCl for record capture and selective separation of NH3. Separation and Purification Technology. **2025**, 374, 133720-133726.

[5] Han, G.; Liu, C.; Yang, Q.; Liu, D.; Zhong, C. Construction of stable IL@MOF composite with multiple adsorption sites for efficient ammonia capture from dry and humid conditions. Chemical Engineering Journal. **2020**, 401, 126106-126112.

[6] Kim, D. W.; Kang, D. W.; Kang, M.; Lee, J.-H.; Choe, J. H.; Chae, Y. S.; Choi, D. S.; Yun, H.; Hong, C. S. High ammonia uptake of a metal-organic framework adsorbent in a wide pressure range. **2020**, 59, 22531-22536.

[7] Kim, D. W.; Kang, D. W.; Kang, M.; Choi, D. S.; Yun, H.; Kim, S. Y.; Lee, S. M.; Lee, J.-H.; Hong, C. S. High gravimetric and volumetric ammonia capacities in robust metal-organic frameworks prepared via double postsynthetic modification. Journal of the American Chemical Society. **2022**, 144, 9672-9683.

[8] Rieth, A. J.; Dincă, M. Controlled gas uptake in metal-organic frameworks with record ammonia sorption. Journal of the American Chemical Society. **2018**, 140, 3461-3466.

[9] Wang, Z.; Li, Z.; Zhang, X.-G.; Xia, Q.; Wang, H.; Wang, C.; Wang, Y.; He, H.; Zhao, Y.; Wang, J. Tailoring multiple sites of metal-organic frameworks for highly efficient and reversible ammonia adsorption. ACS Applied Materials & Interfaces. **2021**, 13, 56025-56034.

[10] Wang, Y.; Shi, Y.; Xiong, D.; Li, Z.; Wang, H.; Xuan, X.; Wang, J. Metal chloride functionalized MOF-253(Al) for high-efficiency selective separation of ammonia from H2 and N2. Chemical Engineering Journal. **2023**, 474, 145307-145316.

[11] Cao, R.; Chen, Z.; Chen, Y.; Idrees, K. B.; Hanna, S. L.; Wang, X.; Goetjen, T. A.; Sun, Q.; Islamoglu, T.; Farha, O. K. Benign integration of a Zn-azolate metal-organic framework onto textile fiber for ammonia capture. ACS Applied Materials & Interfaces. **2020**, 12, 47747-47753.

[12] Snyder, B. E. R.; Turkiewicz, A. B.; Furukawa, H.; Paley, M. V.; Velasquez, E. O.; Dods, M. N.; Long, J. R. A ligand insertion mechanism for cooperative NH3 capture in metal-organic frameworks. Nature. **2023**, 613, 287-291.

[13] Chen, Y.; Shan, B.; Yang, C.; Yang, J.; Li, J.; Mu, B. Environmentally friendly synthesis of flexible MOFs M(NA)2 (M = Zn, Co, Cu, Cd) with large and regenerable ammonia capacity. Journal of Materials Chemistry A. **2018**, 6, 9922-9929.

[14] Han, X.; Lu, W.; Chen, Y.; da Silva, I.; Li, J.; Lin, L.; Li, W.; Sheveleva, A. M.; Godfrey, H. G. W.; Lu, Z.; et al. High ammonia adsorption in MFM-300 materials: dynamics and charge transfer in host-guest binding. Journal of the American Chemical Society. **2021**, 143, 3153-3161.

[15] Chen, Y.; Du, Y.; Liu, P.; Yang, J.; Li, L.; Li, J. Removal of ammonia emissions via reversible structural Transformation in M(BDC) (M = Cu, Zn, Cd) metal-organic frameworks. Environmental

Science & Technology. **2020**, 54, 3636-3642.
[16] Ma, Y.; Lu, W.; Han, X.; Chen, Y.; da Silva, I.; Lee, D.; Sheveleva, A. M.; Wang, Z.; Li, J.; Li, W.; et al. Direct observation of ammonia storage in UiO-66 incorporating Cu(II) binding sites. Journal of the American Chemical Society. **2022**, 144, 8624-8632.
[17] Spanopoulos, I.; Xydias, P.; Malliakas, C. D.; Trikalitis, P. N. A straight forward route for the development of metal-organic frameworks functionalized with aromatic -OH Groups: synthesis, characterization, and gas (N2, Ar, H2, CO2, CH4, NH3) sorption properties. Inorganic Chemistry. **2013**, 52, 855-862.
[18] Rieth, A. J.; Tulchinsky, Y.; Dinca, M. High and reversible ammonia uptake in mesoporous azolate metal organic frameworks with open Mn, Co, and Ni sites. Journal of the American Chemical Society. **2016**, 138, 9401-9404.
[19] Chen, Z.; Wang, X.; Cao, R.; Idrees, K. B.; Liu, X.; Wasson, M. C.; Farha, O. K. Water-based synthesis of a stable iron-based metal-organic framework for capturing toxic gases. ACS Materials Letters. **2020**, 2, 1129-1134.
[20] Lyu, P.; Wright, A. M.; Lopez-Olvera, A.; Mileo, P. G. M.; Antonio Zarate, J.; Martinez-Ahumada, E.; Martis, V.; Williams, D. R.; Dinca, M.; Ibarra, I. A.; et al. Ammonia capture via an unconventional reversible guest-induced metal-linker bond dynamics in a highly stable metal-organic framework. Chemistry of Materials. **2021**, 33, 6186-6192.